

Towards Function Space Mesh Watermarking: Protecting the Copyright of Signed Distance Fields

Xingyu Zhu^{1,2} Guanhui Ye¹ Chengdong Dong² Xiapu Luo² Xuetao Wei^{1*}

¹Southern University of Science and Technology

²Hong Kong Polytechnic University

{12150086, 12132370}@email.sustech.edu.cn, chengdong.dong@connect.polyu.hk
csxluo@comp.polyu.edu.hk, weixt@sustech.edu.cn

Abstract

The signed distance field (SDF) represents 3D geometries in continuous function space. Due to its continuous nature, explicit 3D models (e.g., meshes) can be extracted from it at arbitrary resolution, which means losing the SDF is equivalent to losing the mesh. Recent research has shown meshes can also be extracted from SDF-enhanced neural radiance fields (NeRF). Such a signal raises an alarm that any implicit neural representation with SDF enhancement can extract the original mesh, which indicates identifying the SDF’s intellectual property becomes an urgent issue. This paper proposes **FuncMark**, a robust and invisible watermarking method to protect the copyright of signed distance fields by leveraging analytic on-surface deformations to embed binary watermark messages. Such deformation can survive isosurfacing and thus be inherited by the extracted meshes for further watermark message decoding. Our method can recover the message with high-resolution meshes extracted from SDFs and detect the watermark even when mesh vertices are extremely sparse. Furthermore, our method is robust even when various distortions (including remeshing) are encountered. Extensive experiments demonstrate that our **FuncMark** significantly outperforms state-of-the-art approaches and the message is still detectable even when only 50 vertex samples are given.

1. Introduction

The signed distance field (SDF) is an implicit neural representation representing high fidelity 3D geometry [6, 19, 21, 24, 30, 35, 40, 43, 52]. With a SDF, we can extract meshes with arbitrary resolutions through isosurfacing [10, 17, 25, 32, 41, 42], which means losing the signed distance field is almost equivalent to losing the original mesh. Recent research [11, 31, 47] also enhanced neural

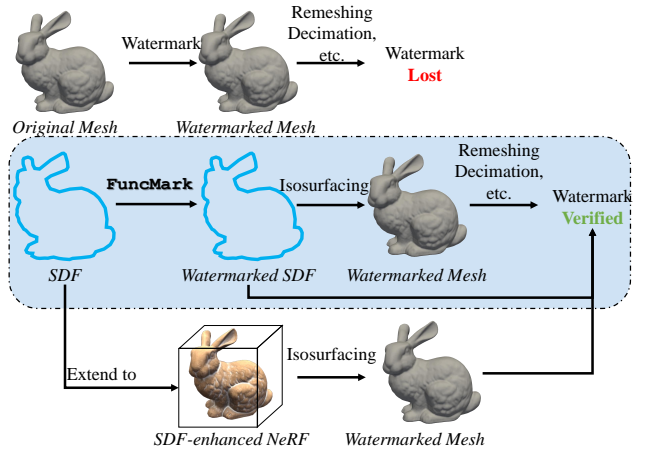


Figure 1. The relationship among signed distance field (SDF), mesh watermarking, and SDF-enhanced NeRF. **Top:** traditional mesh watermarking protects discretized meshes but fails to withstand remeshing and decimation. **Middle:** our method watermarks SDF (i.e. mesh in function space), which can survive remeshing, and decimation. **Bottom:** SDF can be extended to NeRF as geometry enhancement, and our method protects the geometry copyright of SDF-enhanced NeRF.

radiance field (NeRF) by introducing SDF into geometry representation, and such SDF-enhanced NeRF also can extract meshes [20, 31, 39]. Such signal raises an alarm: *any SDF-enhanced implicit neural field has the potential to extract original meshes, which indicates identifying the SDF’s intellectual property becomes an urgent issue*. Thus, the research question in our paper is: *how to protect the copyright of signed distance fields?*

We highlight connections and differences between our work and previous work (including mesh watermarking and NeRF watermarking) in Fig. 1. For mesh watermarking, the significance of the copyright of meshes has been noticed for decades [14–16, 33, 46, 49, 51, 54]. However, these work protected discretized meshes and thus could not

*Corresponding Author

withstand remeshing and resolution changes (*e.g.*, decimation). For NeRF watermarking, CopyRNeRF [26] embedded secret messages into NeRF by replacing the original color representation with a watermarked color representation. However, CopyRNeRF ignored recent advances in SDF-enhanced NeRF [11, 20, 31, 39, 47], leaving the geometry of implicit neural representation unprotected. In this case, a malicious user can bypass watermark verification by extracting meshes instead of rendering images. The stolen mesh can be reused to train completely non-watermarked implicit neural fields. We notice such research gaps and propose to protect the copyright of the signed distance field and its extracted meshes.

Our goal is to watermark both signed distance fields (SDFs) and meshes extracted from them. SDFs represent 3D surfaces with a level set of a field: $\mathcal{S} = \{\mathbf{x} | F(\mathbf{x}) = c\}$. Different from NeRF [29], which represents 3D scenes by mapping viewports to rendered images, SDFs represent accurate 3D surfaces with high-frequency details by mapping 3D coordinates to signed distance from 3D surfaces.

An intuitive solution is directly watermarking the extracted 3D meshes using digital watermarking [14, 37, 46, 51]. However, this only protects the copyright of extracted meshes, leaving the SDF unprotected. Malicious users who steal the SDF may extract new meshes with different resolutions or isosurfacing methods, leaving no room for external watermarking expected by SDF creators. Another option is first to watermark a 3D mesh and then create SDF from the watermarked 3D mesh. Such a method introduces too many geometry differences between the watermarked and original SDF, leading to a noticeable degradation in mesh quality.

In this paper, we propose **FuncMark**, the first signed distance field (SDF) watermarking method, which can verify the ownership of both signed distance fields and 3D meshes extracted from them. Compared to traditional digital watermarking [14, 37, 46, 51], our method is a continuous function space watermark that focuses on 3D surfaces instead of discretized meshes. Compared to previous NeRF watermarking [26], our method is a novel watermarking pipeline designed for a completely different category of implicit neural fields. Our proposed method embeds secret messages in SDFs through spherical partitioning and local deformation. Spherical partitioning divides 3D space into multiple partitions to embed one bit in each partition. The local deformation is analytically performed within each partition based on the bit embedded in the current partition. Such deformation is made directly on 3D surfaces without discretization and can be further analyzed to recover the embedded secret messages. By doing so, 3D meshes extracted from SDFs inherit such deformation and can be applied for further message decoding. Due to the nature of function space watermarking, our method is robust against notorious remeshing attacks, which has been an open issue for pre-

vious digital watermarking methods. Besides, our experiments show that our method is also robust against other various mesh distortions, such as Gaussian noise, affine transformation, simplification, smoothing, and quantization. We summarize our contributions as the following:

- We propose the first, to the best of our knowledge, robust and invisible watermarking method **FuncMark** to protect the copyright of signed distance fields.
- We propose to embed secret messages through spherical partitioning and analytic message-guided deformation without discretization. The deformation is achieved analytically instead of using RELU-based neural networks, which enables the resultant SDF to remain a valid signed distance function. In the decoding phase, we devise rigorous watermark decoding and detection methods, where decoding is for dense mesh vertices and detection is for sparse mesh vertices.
- We conduct extensive experiments to show that our **FuncMark** significantly outperforms state-of-the-art approaches and the watermark is detectable even when mesh vertices are extremely sparse (around 50 vertices). Furthermore, our **FuncMark** can withstand various mesh distortions, such as Gaussian noise, affine transformation, simplification, smoothing, quantization, and remeshing.

2. Related Work

2.1. Implicit Neural Representations

Implicit neural representation represents continuous 3D signals parameterized by multi-layer perceptrons (MLPs). Signed distance fields represents accurate 3D shapes by mapping 3D coordinates to geometry values such as occupancy value [27, 38] or signed distance functions [3, 4, 6, 8, 11, 21, 28, 35, 43, 52]. SIREN [43] pioneeringly applied sine transform to the input coordinates, enabling SDFs to better represent high-frequency details. These approaches are supervised by a collection of 3D coordinates and ground truth geometry values. Due to the continuous nature of 3D surfaces, meshes at arbitrary resolutions can be extracted from them through isosurfacing. Mildenhall *et al.* [29] first introduced NeRF with its geometry represented by a density function. Recent advances [11, 47] in NeRF have introduced signed distance functions into NeRF to enhance its geometry representation. Further research [20, 31, 39] have extracted high fidelity 3D meshes from SDF-enhanced NeRFs.

2.2. Watermark

There are various research on digital watermarking for explicit 3D meshes. Early research [2, 33, 34] leveraged Fourier and wavelet analysis to transfer meshes into the frequency domain and embedded watermark bits into Fourier/wavelet coefficients. Other approaches [14, 16, 37,

[46, 51] embedded binary messages into vertex coordinate bits. Hou *et al.* [15] introduced a 3D watermarking method by leveraging layer artifacts of 3D printed meshes. [49] leveraged deep neural network to embed messages in 3D meshes and extracted them from rendered images. [54] proposed a deep learning based 3D-to-3D watermark while watermarking discretized meshes instead of continuous 3D surfaces.

Recently, Luo *et al.* [26] watermarked NeRF models by replacing the original color representation in NeRF with a watermarked color representation, but leaving the geometry of implicit neural representation unprotected.

2.3. Isosurfacing

Isosurfacing methods extract a polygon mesh representing the level set of a scalar function, which has been studied extensively across several fields. Marching Cubes (MC) [25], Dual Contouring (DC) [17] and Dual Marching Cubes (DMC) [32] are spatial decomposition methods which divided the space into cells like cubes or tetrahedrons and created polygons within the cells that contain the surface. Neural Marching Cubes (NMC) [9] and Neural Dual Contouring (NDC) [10] proposed a data-driven approach to position the extracted mesh as a function of the input field. DMTet [41] and Flexicubes [42] utilized a differentiable method to extract the mesh.

3. Preliminaries & Definition

Signed distance function (sdf). Let Ω be a set in \mathbb{R}^3 , and $\mathcal{S} = \partial\Omega$ be its boundary. $sdf F : \mathbb{R}^3 \mapsto \mathbb{R}$ maps 3D locations \mathbf{x} to a scalar which represents the signed shortest distance to the 3D surface \mathcal{S} , with its first derivative representing the outward-oriented surface normal. Given a mesh \mathcal{M} with vertex set V , all vertices $v \in V$ satisfy $F(v) = 0$, and $\nabla F(v)$ equals to the vertex normal at vertex v .

Signed Distance Field (SDF) $F_\Theta : \mathbb{R}^3 \mapsto \mathbb{R}$ parameterizes continuous signals for 3D objects. A handy parameterization of sdf function uses a fully-connected neural network with the following unified formulation:

$$\begin{aligned} F_\Theta(\mathbf{x}) &= \mathbf{W}_n(f_{n-1} \circ f_{n-2} \circ \dots \circ f_1)(\mathbf{x}) \\ f_i(\mathbf{x}) &= \sigma_i(\mathbf{W}_i\mathbf{x} + \mathbf{b}_i) \end{aligned} \quad (1)$$

where $\mathbf{W}_i, \mathbf{b}_i$ are the weight matrix and bias of the i -th layer, and σ_i is an element-wise nonlinear activation function. σ_i is either ReLU [3, 28, 35] or sinusoidal function used in SIREN[43]. Due to the smooth nature of sinusoidal functions, SIREN can approximate both $F(\mathbf{x})$ and $\nabla F(\mathbf{x})$, where $F_\Theta(\mathbf{x})$ is supervised with ground truth values for $\mathbf{x} \in \mathbb{R}^3$ while $\nabla F(\mathbf{x})$ is supervised only by the \mathbf{x} on zero-isosurface.

Isosurfacing can extract c -isosurface from a given scalar function at arbitrary resolution. The c -isosurface on the sdf

function is defined as $\mathcal{S} = \{\mathbf{x} | F(\mathbf{x}) = c\}$. The zero-isosurface is extracted from the sdf function as meshes. Some isosurfacing methods, such as Dual Contouring [17], require surface normal information to extract 3D meshes, which adds another reason for us to select SIREN as the backbone for the concern of flexible choice of isosurfacing methods.

4. Method

Our goal is to watermark both SDF and meshes extracted from them. In embedding phase, the owner embeds a binary message $\mathbf{M} \in \{0, 1\}^{N_m}$ in SDF F_Θ to get the watermarked SDF G_Θ . In the ownership verification phase, we expect the following application scenarios:

- **Watermark decoding.** The investigator can decode the message from the given media to trace the leaker.
- **Watermark detection.** When the investigator cannot decode the complete message, he/she can still detect the watermark according to a statistical measure.

The media mentioned above can be either an SDF (white-box scenario) or a mesh extracted from an SDF (black-box scenario). In practice, we select SIREN [43] as our SDF backbone because our method requires accurate approximation on both $F(x)$ and $\nabla F(x)$.

To design a watermarking scheme satisfying both white-box and black-box scenarios, we embed binary messages \mathbf{M} in the output of F_Θ through local deformations of implicit neural representations. In detail, we apply our watermarking embedding process as the following pipeline: (1) we first divide 3D space and SDF into $N_s * N_s$ partitions under the spherical coordinate system (Sec. 4.1); (2) within each partition we embed one bit b , and we deform the partition according to b (Sec. 4.2); (3) we design two measures for decoding process to verify the ownership for both white-box and black-box scenarios (Sec. 4.3).

4.1. Spherical Partitioning

Our first step is to divide 3D space under a spherical coordinate system since we only embed one bit in each partition. A spherical coordinate system is a coordinate system for three-dimensional space where the position of a given point in space is specified by three numbers (r, θ, ϕ) , where r is the length of radial line connecting the point to the origin, $\theta \in [0, \pi]$ is measured by the angle between z-axis and the radial line, and $\phi \in [-\pi, \pi]$ is measured by the angle between x-axis and the orthogonal projection of the radial line onto the reference x-y plane.

A cartesian coordinate (x, y, z) and spherical coordinate

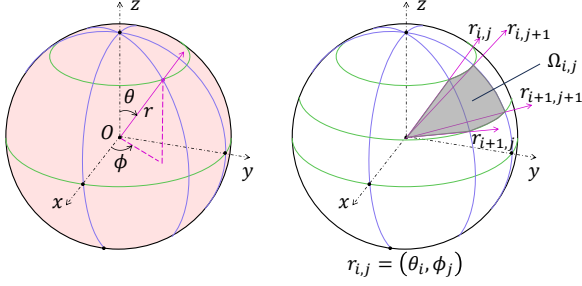


Figure 2. **Left:** a spherical system where points are represented in coordinate (r, θ, ϕ) . **Right:** a spherical partition $\Omega_{i,j}$, which contains all points bounded by axis $r_{i,j}, r_{i,j+1}, r_{i+1,j}, r_{i+1,j+1}$.

(r, θ, ϕ) can be converted to each other by the following:

$$\begin{cases} r = \sqrt{x^2 + y^2 + z^2} \\ \theta = \arccos(\frac{z}{r}) \\ \phi = \arctan(\frac{y}{x}) \end{cases} \quad \begin{cases} x = r \sin(\theta) \cos(\phi) \\ y = r \sin(\theta) \sin(\phi) \\ z = r \cos(\theta) \end{cases} \quad (2)$$

We divide 3D space by equally dividing θ and ϕ into N_s parts. In this case, the implicit neural representation is also divided into $N_s * N_s$ parts. A spherical partition $\Omega_{i,j}$ is a local region $\{(r, \theta, \phi) | \theta \in [\theta_i, \theta_{i+1}] \cap \phi \in [\phi_j, \phi_{j+1}]\}$. Ideally, we expect the zero-iso-surface to be evenly divided by each partition, so we normalize all meshes within a unit sphere before we build non-watermarked SDFs F_Θ .

4.2. Watermark Embedding

Overview. Our watermark is embedded by introducing independent deformations in each partition. To deform an SDF F_Θ , we wrap the coordinate space of F_Θ using an analytic deformation function $D(\mathbf{y})$, which deforms a point \mathbf{y} to $\mathbf{x} = D(\mathbf{y})$. Under this framework, the deformed SDF G_Θ can be represented as $G_\Theta(\mathbf{x}) = F_\Theta(D^{-1}(\mathbf{x}))$ [12, 23, 48]. We expect the following two properties: **(1)** D is continuous and invertible, so that $G_\Theta(\mathbf{x})$ can be calculated for $\mathbf{x} \in \mathbb{R}^3$; **(2)** G_Θ is still an *sdf*, i.e., G_Θ and $\nabla G(\mathbf{x})$ are valid signed distance values and normal vectors, respectively, so that G_Θ can be still applied to downstream tasks. After achieving both properties, the final step is to remove the reliance of $D^{-1}(\mathbf{x})$ because malicious users can remove the watermark by removing $D^{-1}(\mathbf{x})$. We achieve this by distilling $F_\Theta(D^{-1}(\mathbf{x}))$ with a brand new SIREN network.

Define $D(\mathbf{y})$. After dividing SDF into $N_s * N_s$ partitions along with the subdivision of 3D space in Sec. 4.1, the next step is to make deformation within each partition to embed a binary bit. The deformation function $D(\mathbf{y})$ is defined within each region. Consider a partition embedded with a bit b , for

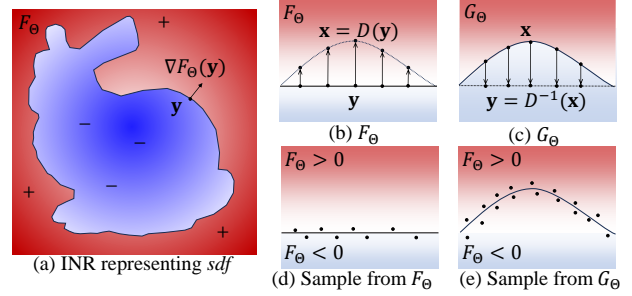


Figure 3. We show a SDF in (a). Within a partition embedded with bit b , we build one-to-one correspondence between original points \mathbf{y} and watermarked points \mathbf{x} . (b-c) visualize the watermarking process when $b = 1$, and (c) shows the watermarked SDF G_Θ . In (d-e), we sample around zero-iso-surface of F_Θ, G_Θ , respectively. In (e), the number of positive samples are significantly more than the number of negative ones, and thus, we reject the null hypothesis and detect the watermark.

all $\mathbf{y} \in \Omega_{i,j}$,

$$D(\mathbf{y}) = \begin{cases} \mathbf{y} + \nabla F_\Theta(\mathbf{y})C(\mathbf{y}) & b = 1 \\ \mathbf{y} - \nabla F_\Theta(\mathbf{y})C(\mathbf{y}) & b = 0 \end{cases} \quad (3)$$

where $C : \mathbb{R}^3 \mapsto \mathbb{R}$ is a scalar function (C will be defined later). $D(\mathbf{y})$ moves \mathbf{y} along the direction of surface normal $\nabla_{\mathbf{y}} F_\Theta$ with moving length $C(\mathbf{y})$ if $b = 1$, otherwise moves \mathbf{y} against the direction of surface normal. For convenience, we denote the operation that moves a point along the direction of its normal vector as **outward** and denote the operation that moves a point against the direction of its normal as **inward**. We show the visualized process in Fig. 3 (b-c). We expect $C(\mathbf{y})$ to be smaller when $\mathbf{y} \in \Omega_{i,j}$ is close to the edge of $\Omega_{i,j}$. We achieve such feature by defining $C(\mathbf{y})$ as following:

$$C(\mathbf{y}) = 16\delta \frac{(\theta_{i+1} - \theta_{\mathbf{y}})(\theta_{\mathbf{y}} - \theta_i)}{(\theta_{i+1} - \theta_i)^2} \frac{(\phi_{j+1} - \phi_{\mathbf{y}})(\phi_{\mathbf{y}} - \phi_j)}{(\phi_{j+1} - \phi_j)^2} \quad (4)$$

where δ is a constant parameter representing the watermarking strengths.

Make D invertible. One way to make D invertible is to approximate D with invertible residual blocks [48]. However, in practice, we find the accuracy of invertible residual blocks cannot satisfy the accuracy requirements of watermarking. Besides, invertible residual blocks are ReLU-based networks, which make it hard to approximate both *sdf* values and surface normals [43].

Newton’s method calculates $D^{-1}(\mathbf{x})$. $\mathbf{y} = D^{-1}(\mathbf{x})$ cannot be written in an analytic formula, since $\nabla F_\Theta(\mathbf{y})$ has no analytic formula. Fortunately, we can still derive $\mathbf{y} = D^{-1}(\mathbf{x})$ by calculating the zero point of $\mathbf{y} \pm \nabla F_\Theta(\mathbf{y})C(\mathbf{y}) - \mathbf{x} = 0$. We apply Newton’s method [50] to calculate the

zero point as the following repeated process:

$$\mathbf{y}_{n+1} = \mathbf{y}_n - \mathcal{J}_D^{-1}(\mathbf{y}_n) \cdot D(\mathbf{y}_n) \quad (5)$$

where \mathbf{y}_i is the guessed zero point at i -th iteration, \cdot is the matrix multiplication operation, and $\mathcal{J}_D^{-1}(\mathbf{y})$ is the inverse of Jacobian matrix of D at the point \mathbf{y} . To calculate a correct zero point, this process is sensitive to the accuracy of $\mathcal{J}_D(\mathbf{y})$, which is derived from Hessian of the SDF: $\mathcal{H}_{F_\Theta}(\mathbf{y})$ (We show details in Supplementary Sec. A). However, $\nabla F_\Theta(\mathbf{y})$ is supervised with ground truth value only when \mathbf{y} is on zero-isosurface. Thus, Newton’s method may not find a zero point if the initialization y_0 is far from the zero-isosurface. We randomly initialize multiple y_0 within $[-1, 1]^3$ to alleviate this issue. We find that 100 samples are enough to find the ground truth zero point.

$\nabla G_\Theta(\mathbf{x})$ can be derived in an analytic way: $\nabla G_\Theta(\mathbf{x}) = \mathcal{J}_{D^{-1}}(\mathbf{x}) \cdot \nabla F(\mathbf{y})$, where $\mathbf{y} = D^{-1}(\mathbf{x})$, and $\mathcal{J}_{D^{-1}}(\mathbf{x})$ can be derived directly from Eq. (3) (We show details in Supplementary Sec. A):

$$\mathcal{J}_{D^{-1}}(\mathbf{x}) = \left(C(y)\mathcal{H}_{F_\Theta}(y) + \nabla C(y)(\nabla F_\Theta(y))^T + \mathcal{I} \right)^{-1} \quad (6)$$

where $y = D^{-1}(x)$

4.3. Ownership Verification

Tagging points. After dividing SDF into $N_s * N_s$ partitions, we decode each bit independently within each partition. As shown in Fig. 3 (d-e), for all points $\mathbf{x} \in \Omega_{i,j}$, we tag point \mathbf{x} with bit 1 if $F_\Theta(\mathbf{x}) > 0$, otherwise we tag it with bit 0. Remember that we have white-box and black-box ownership declaration scenarios. In the black-box ownership declaration scenario, a mesh \mathcal{M} is given to evaluate whether the mesh is generated from the watermarked SDF. In this case, we directly tag its vertex set V with the binary bit. In the white-box ownership declaration scenario where an SDF is given, we can either extract a mesh from it through iso-surfacing or sampling points on the zero-isosurface of the SDF. We use the same sampling strategy in [48] where they sample points from a rough shape and then apply Langevin dynamics to get an accurate sample on zero-isosurface. We denote N_v as the number of vertices of the mesh or the number of sampled points on zero-isosurface.

Measure. Ideally, we expect all regions to have some points to decode the bit embedded in that region. However, when N_s is large, and N_v is small, it is possible that no points lie in a specific partition. In this case, that partition cannot be decoded. We design two measures for ownership verification: watermark decoding for dense points and watermark detection for sparse points.

- **Watermark decoding.** A partition is tagged with bit b if more than half of the points in that region is tagged with bit b . In this case, we can get a decoded message $\hat{\mathbf{M}}$, which can be compared with \mathbf{M} with bit accuracy.

- **Watermark detection.** We say the point matches the partition it belongs to if the tagged bit matches the bit embedded in that region. In the case of sparse points, we detect the watermark by testing the following hypothesis [18].

$$H_0 : \text{the implicit neural fields/mesh is generated} \quad (7)$$

without knowledge of the secret message \mathbf{M} .

If the null hypothesis is true, the number of points that match their partition, denoted as s , has an expected value $N_v/2$ and variance $N_v/4$. The z -statistic for this test is

$$z = 2(s - N_v/2)/\sqrt{N_v} \quad (8)$$

We reject the null hypothesis when z is above a threshold given a significance level α .

How hard is it to remove the watermark? We evaluate robustness against classic mesh attacks, including Gaussian noise, affine transformation and remeshing. We find that Gaussian noise cannot remove our watermark unless the distortion made by Gaussian noise severely damages the visual effect. Affine transformation can remove the watermark easily because all points will be tagged by a wrong bit. To alleviate this issue, we align the given mesh (with vertex set V) with watermarked SDF G_Θ by minimizing:

$$(a^*, \beta^*, \theta^*, \phi^*, \mathbf{t}^*) = \arg \min_{a, \beta, \theta, \phi, \mathbf{t}} \sum_{v \in V} \|G_\Theta(a\mathbf{R}(\beta, \theta, \phi)v + \mathbf{t})\| \quad (9)$$

where a is the scaling factor, $\mathbf{R}(\beta, \theta, \phi)$ representing the function mapping a rotation angle β and a rotation axis (θ, ϕ) to the rotation matrix, and \mathbf{t} is the translation vector. 3D rotation learning is hard due to the non-continuous mapping of \mathbf{R} [53]. Gradient descent can find the global optimum only if the initialized parameter set $(\alpha, \beta, \theta, \phi, \mathbf{t})$ is close to optimum $(\alpha^*, \beta^*, \theta^*, \phi^*, \mathbf{t}^*)$. We perform a coarse-to-fine grained parameter search. For coarse-grained search, we use grid search to find a set of initialized parameter set $(\alpha, \beta, \theta, \phi, \mathbf{t})$. For fine-grained search, we use gradient descent within each grid to find the global optimum.

5. Evaluation

5.1. Setup

We implement SIREN using four layers of MLPs with 256 channels to build both F_Θ and G_Θ . Since we embed each spherical partition with one binary bit in the secret message \mathbf{M} , if the number of partitions $N_s * N_s$ is greater than the length of the message, we repeatedly embed messages until we consume all partitions. Unless explicitly mentioned, our experiment is conducted under the following settings. We set $N_s = 32$ (i.e. the spherical system is divided into $32 * 32$ partitions). The default embedded message has a 16-bit length. We select significance level $\alpha = 0.001$. In

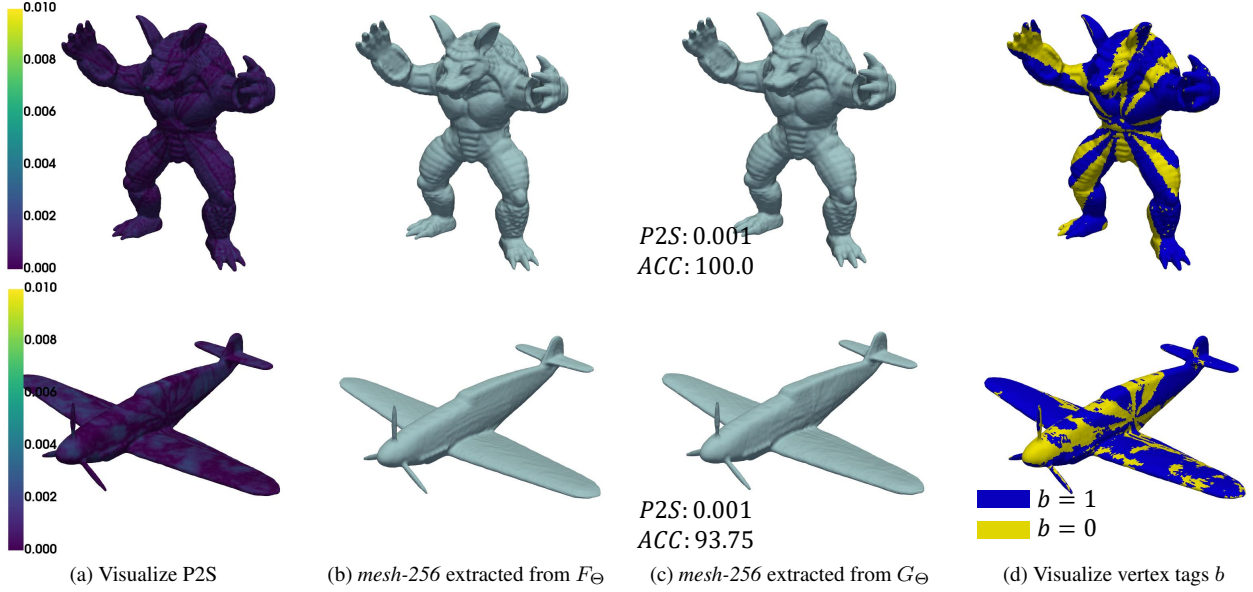


Figure 4. (a-c) Visualize geometric differences between $mesh-256$ from F_Θ and G_Θ . (d) Vertex tags b on $mesh-256$ from G_Θ .

Methods	Verify on	8-bit				16-bit				32-bit			
		CD↓	P2S↓	Normal↓	Acc↑	CD↓	P2S↓	Normal↓	Acc↑	CD↓	P2S↓	Normal↓	Acc↑
<i>deform-mesh</i>	<i>mesh-64</i>	0.060	0.052	0.2014	73.00	0.058	0.047	0.1924	69.84	0.050	0.035	0.1824	67.61
	<i>mesh-128</i>	0.051	0.049	0.1778	81.80	0.049	0.044	0.1728	85.56	0.043	0.031	0.1561	80.78
	<i>mesh-256</i>	0.049	0.048	0.1723	89.88	0.047	0.043	0.1630	88.70	0.040	0.030	0.1488	89.21
	G_Θ	/	0.021	/	91.21	/	0.018	/	92.18	/	0.022	/	90.17
FuncMark	<i>mesh-64</i>	0.004	0.006	0.1065	82.90	0.004	0.006	0.1052	79.85	0.005	0.006	0.1125	75.75
	<i>mesh-128</i>	0.003	0.004	0.0865	90.60	0.003	0.004	0.0871	87.56	0.003	0.005	0.0917	82.00
	<i>mesh-256</i>	0.002	0.004	0.0828	95.69	0.003	0.004	0.0833	93.12	0.003	0.004	0.0889	94.37
	G_Θ	/	0.002	/	94.34	/	0.002	/	94.31	/	0.002	/	94.60

Table 1. Performance comparison with *deform-mesh*. Note that “/” means that CD and Normal differences cannot be used to measure the geometric distance between sampled points and a surface. This table shows that (1) *deform-mesh* makes $9\times$ more geometry differences than **FuncMark**, resulting in lower mesh quality; (2) decoding accuracy drops when isosurfacing resolution r decreases; (3) message lengths have little effects on both geometry difference and decoding accuracy.

this case, we reject the H_0 hypothesis when $z > 3.09$ with a false positive probability of 10^{-3} . We use marching cube [25] as our default isosurfacing method and the default watermarking strength $\delta = 0.001$.

Dataset. To create a set of origin implicit neural fields, we use mesh fusion [44] to create watertight meshes from ShapeNet [7] and Stanford Repo [1]. All watertight meshes are normalized to the unit sphere. We further uniformly sample five million points on mesh surface where their sdf values are zero and another five million points on $[-1, 1]^3$ where their sdf values are estimated following the same process in [48]. We then fit F_Θ [43] to the ground truth sdf , and ∇F_Θ to vertex normals.

Baselines. We first compare **FuncMark** with prior classic watermarking methods [2, 16, 36, 45] which focused on discretized meshes. Since there is no function space mesh

watermarking, we then design a rigorous baseline *deform-mesh*, which makes deformations on a mesh instead of SDF: (1) perform spherical partitioning as is in Sec. 4.1, (2) deform mesh vertices inward/outward with respect to the bit embedded in their belonging partitions, (3) fitting G_Θ from the watermarked meshes.

Evaluation Methodology. We verify the watermark on both watermarked SDF (white-box) and meshes extracted from it (black-box). For convenience, a mesh extracted in resolution r through isosurfacing methods will be denoted as *mesh-r*. We aim to evaluate geometry differences (Chamfer distance, P2S distance, and Normal difference) and watermark accuracy (z -score and bit accuracy). Chamfer distance (CD) computes average bi-directional point-to-point distances, capturing large geometry differences but missing smaller geometric details. P2S distance computes

Methods	Geometry Difference↓		Accuracy & Robustness↑					
	CD	Normal	w/o attack	Gaussian	Rotation	Translation	Remesh	Decimate
Jiang <i>et al.</i> [16]	0.009	0.0859	80.59	76.98	80.58	48.21	50.21	49.16
Hiba <i>et al.</i> [2]	0.012	0.1195	87.48	54.31	50.40	50.41	52.35	51.50
Tsai <i>et al.</i> [45]	0.085	0.2272	91.41	50.03	49.75	49.99	51.48	50.48
Peng <i>et al.</i> [36]	0.009	0.0873	91.98	50.24	50.55	58.30	51.46	52.70
FuncMark (Ours)	0.002	0.0828	95.69	95.69	82.44	93.12	92.41	91.13

Table 2. Performance comparison with traditional mesh watermarking methods, which watermark discretized meshes.

sampling N_v	$\delta = 0.0010$			$\delta = 0.0005$		
	precision	recall	F1 score	precision	recall	F1 score
10	1.00	0.422	0.593	1.00	0.133	0.235
50	1.00	0.978	0.989	1.00	0.656	0.792
100	1.00	1.00	1.00	1.00	0.833	0.909
1000	0.968	1.00	0.984	0.988	0.933	0.960
5000	0.978	1.00	0.989	1.00	0.955	0.977

Table 3. Error rate for watermark detection under varied N_v .

δ	Verify on	CD↓	P2S↓	Normal↓	Acc↑
0.0005	<i>mesh-128</i>	0.002	0.004	0.0744	71.85
	G_Θ	/	0.002	/	73.33
0.0010	<i>mesh-128</i>	0.003	0.004	0.871	87.56
	G_Θ	/	0.002	/	94.31

Table 4. Tradeoffs between geometry differences and watermarking accuracy by varying δ . Note that “/” means that CD and Normal differences cannot be used to measure the geometric distance between sampled points and a surface.

the average point-to-surface distance from watermarked points to the original surface. Normal difference computes vertex normal difference between points and their nearest on-surface points, which captures differences for high-frequency geometric details when CD and P2S are small. CD and Normal differences are used to compute geometry differences between *mesh-r* extracted from F_Θ and G_Θ , while P2S is used to evaluate geometry distance between points and surfaces.

5.2. Accuracy

Visual Quality. We visualize meshes extracted from both F_Θ and G_Θ in Fig. 4, where we use point-to-surface (P2S) distance to evaluate geometry differences. Besides, we visualize vertex tags to better understand how secret messages are embedded.

FuncMark vs. Baselines. We conduct two independent experiments to compare the performance between function space watermarking (Tab. 1), and the performance between

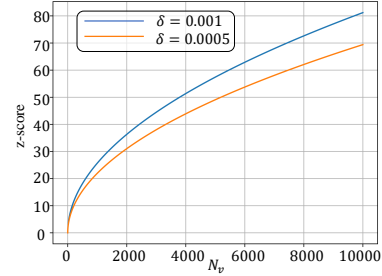


Figure 5. The average z -score as a function of the number of sampled points N_v .

FuncMark and discretized mesh watermarking (Tab. 2). In the first experiment, we compare *deform-mesh* and **FuncMark** under different message lengths in black/white-box scenarios. Under arbitrary verification media, Tab. 1 first shows that *deform-mesh* has lower bit accuracy and makes $9\times$ more geometry differences than **FuncMark**. The reason is that *deform-mesh* embeds a watermark by first deforming meshes and then creating SDFs from watermarked meshes. Mesh deformation and SDF fitting errors make too many geometry differences, while **FuncMark** directly performs accurate deformation on SDFs with low geometry differences. In the second experiment, we compare **FuncMark** and discretized watermarking in Tab. 2. Since prior works only focus on meshes, all evaluations of **FuncMark** are conducted on extracted *mesh-256*. Tab. 2 shows that **FuncMark** outperforms prior methods and shows high robustness against remeshing and decimation attacks.

Bit Accuracy in Watermark Decoding. We evaluate bit accuracy under different resolution r when only extracted *mesh-r* are given (black-box) and different sampling number N_v when G_Θ is given (white-box). In the white-box scenario, we directly sample $N_v = 30000$ points on G_Θ and perform watermark decoding on sampled points. In the black-box scenario, we extract *mesh-r* from G_Θ and perform watermark decoding on mesh vertices. *mesh-64* has averaged $N_v = 2764$ vertices and *mesh-256* has averaged $N_v = 48088$ vertices. Tab. 1 shows that we have 94% bit accuracy when $r = 256$ while accuracy drops fast when points are sparser. This raises a question: can we still detect the watermark even if given vertices are extremely sparse?

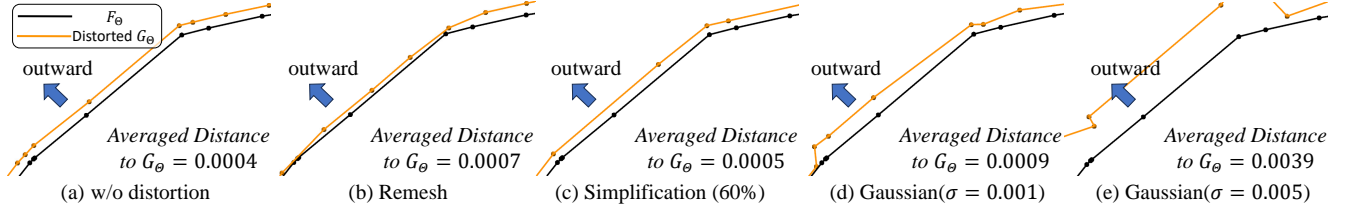


Figure 6. Robustness analysis under $\delta = 0.001$. We show a local region within a partition embedded with $b = 1$ (outward).

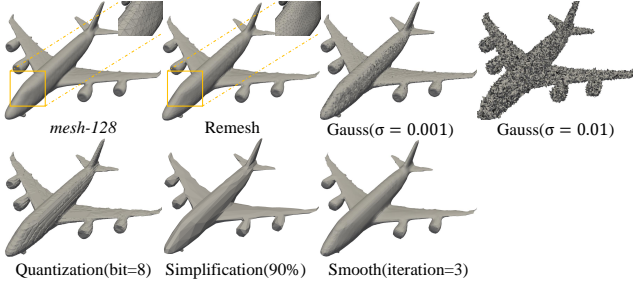


Figure 7. Distorted *mesh-128* after being extracted from G_Θ .

Isosurfacing	Acc
Marching Cubes [25]	93.12
Dual Contouring [17]	87.75
Neural Dual Contouring [10]	88.61
DMTet [41]	89.46

Table 5. Accuracy with different isosurfacing methods.

Distortion	Acc
w/o distortion	94.61
Gaussian($\sigma = 0.001$)	94.61
Gaussian($\sigma = 0.005$)	85.37
Gaussian($\sigma = 0.01$)	64.87
Rotation($\pm\pi$)	82.44
Scaling($< 25\%$)	93.75
Translation	94.61
Combined	76.62
Simplification (30%)	93.75
Simplification (60%)	94.11
Simplification (90%)	76.37
Smoothing (iteration=1)	93.75
Smoothing (iteration=2)	93.12
Smoothing (iteration=3)	78.87
Quantization (bit=16)	93.87
Quantization (bit=12)	91.01
Quantization (bit=8)	65.62
Remeshing	93.46

Table 6. Bit accuracy with different distortion types.

Error Rate in Watermark Detection. We evaluate the error rate under different sampling numbers N_v . We use uniform sampling on the surface. We first show in Fig. 5 that with the increase of N_v , z -score increases, and thus we have more confidence to reject H_0 to detect our watermark. Tab. 3 shows that our watermark can be detected with only $N_v = 50$ sampled points.

Watermark Strength vs. Mesh Quality. We conduct more experiments to evaluate the relationship between bit accuracy and mesh quality, the results of which are shown in Tab. 4. By varying watermarking strength δ , we achieve a good balance between mesh quality and bit accuracy when $\delta = 0.001$.

5.3. Robustness

Robustness on Isosurfacing. The watermark on extracted meshes should be robust against different isosurfacing methods. In Tab. 5, we see our robustness against multiple isosurfacing methods [17, 25, 32, 41].

Robustness on Mesh Attack. Combining Tab. 6 and Fig. 7, we evaluate robustness against distortions on Gaussian Noise, rotation, scaling, translation, simplification [22], Laplacian smoothing [13], quantization, and remesh-

ing [5]. Since the effect of Gaussian noise increases when the bounding box of meshes is smaller, we need to show the visual effect of arbitrary mesh attacks when the watermarked surfaces and extracted meshes are bounded by $[-1, 1]^3$. In Fig. 7, Gaussian($\sigma = 0.001, 0.01$), Quantization(bit=8), simplification(90%) and Smooth(iteration=3) make obvious visual distortions. We observe the high robustness in Tab. 6 that our watermark cannot be removed unless obvious visual distortions have been made. It is worth noting that our method has high robustness against remeshing, which is known as a common challenge in the mesh watermarking domain.

We provide further analysis of robustness. Arbitrary distortions increase the distance from watermarked vertices to G_Θ . In Fig. 6(a), where no distortion has been made, extracted meshes only suffer from distortions caused by isosurfacing. In Fig. 6(b-c), remeshing inserts of points and edges, and decimation [22] performs edge-collapse and points merging. In both cases, newly generated points maintain outward relative to the original surface.

6. Conclusion

In this paper, we have proposed **FuncMark**, which is the first watermarking method to protect the copyright of signed distance fields towards function space mesh watermarking. The secret message bits are embedded through local deformations in each spherical partition. Our **FuncMark** has achieved invisible and robust watermarking, which can withstand various mesh distortions, such as Gaussian noise, affine transformation, simplification, smoothing, quantization, and remeshing. Our extensive experiments have demonstrated that our **FuncMark** significantly outperforms state-of-the-art approaches and the message is still detectable when given vertices are extremely sparse.

References

- [1] The stanford 3d scanning repository. <https://graphics.stanford.edu/data/3dscanrep/>. Accessed 15-July-2023. **6**
- [2] Hiba Al-Khafaji and Charith Abhayaratne. Graph spectral domain blind watermarking. In *IEEE International Conference on Acoustics, Speech and Signal Processing*, pages 2492–2496. IEEE, 2019. **2, 6, 7**
- [3] Matan Atzmon and Yaron Lipman. Sal: Sign agnostic learning of shapes from raw data. In *Proceedings of the IEEE/CVF Conference on Computer Vision and Pattern Recognition*, pages 2565–2574, 2020. **2, 3**
- [4] Matan Atzmon, Niv Haim, Lior Yariv, Ofer Israelov, Haggai Maron, and Yaron Lipman. Controlling neural level sets. *Advances in Neural Information Processing Systems*, 32, 2019. **2**
- [5] Mario Botsch and Leif Kobbelt. A remeshing approach to multiresolution modeling. In *Proceedings of the 2004 Eurographics/ACM SIGGRAPH symposium on Geometry processing*, pages 185–192, 2004. **8**
- [6] Yukang Cao, Kai Han, and Kwan-Yee K Wong. Sesdf: Self-evolved signed distance field for implicit 3d clothed human reconstruction. In *Proceedings of the IEEE/CVF Conference on Computer Vision and Pattern Recognition*, pages 4647–4657, 2023. **1, 2**
- [7] Angel X. Chang, Thomas Funkhouser, Leonidas Guibas, Pat Hanrahan, Qixing Huang, Zimo Li, Silvio Savarese, Manolis Savva, Shuran Song, Hao Su, Jianxiong Xiao, Li Yi, and Fisher Yu. ShapeNet: An Information-Rich 3D Model Repository. Technical Report arXiv:1512.03012 [cs.GR], Stanford University — Princeton University — Toyota Technological Institute at Chicago, 2015. **6**
- [8] Zhiqin Chen and Hao Zhang. Learning implicit fields for generative shape modeling. In *Proceedings of the IEEE/CVF Conference on Computer Vision and Pattern Recognition*, pages 5939–5948, 2019. **2**
- [9] Zhiqin Chen and Hao Zhang. Neural marching cubes. *ACM Transactions on Graphics (TOG)*, 40(6):1–15, 2021. **3**
- [10] Zhiqin Chen, Andrea Tagliasacchi, Thomas Funkhouser, and Hao Zhang. Neural dual contouring. *ACM Transactions on Graphics (TOG)*, 41(4):1–13, 2022. **1, 3, 8**
- [11] Zhang Chen, Zhong Li, Liangchen Song, Lele Chen, Jingyi Yu, Junsong Yuan, and Yi Xu. Neurf: A neural fields representation with adaptive radial basis functions. In *Proceedings of the IEEE/CVF International Conference on Computer Vision*, pages 4182–4194, 2023. **1, 2**
- [12] Yu Deng, Jiaolong Yang, and Xin Tong. Deformed implicit field: Modeling 3d shapes with learned dense correspondence. In *Proceedings of the IEEE/CVF Conference on Computer Vision and Pattern Recognition*, pages 10286–10296, 2021. **4**
- [13] Mathieu Desbrun, Mark Meyer, Peter Schroder, and Alan H Barr. Implicit fairing of irregular meshes using diffusion and curvature flow. In *Seminal Graphics Papers: Pushing the Boundaries, Volume 2*, pages 149–156, 2023. **8**
- [14] Gangyang Hou, Bo Ou, Min Long, and Fei Peng. Separable reversible data hiding for encrypted 3d mesh models based on octree subdivision and multi-msb prediction. *IEEE Transactions on Multimedia*, 2023. **1, 2**
- [15] Jong-Uk Hou, Do-Gon Kim, and Heung-Kyu Lee. Blind 3d mesh watermarking for 3d printed model by analyzing layering artifact. *IEEE Transactions on Information Forensics and Security*, 12(11):2712–2725, 2017. **3**
- [16] Ruiqi Jiang, Hang Zhou, Weiming Zhang, and Nenghai Yu. Reversible data hiding in encrypted three-dimensional mesh models. *IEEE Transactions on Multimedia*, 20(1):55–67, 2017. **1, 2, 6, 7**
- [17] Tao Ju, Frank Losasso, Scott Schaefer, and Joe Warren. Dual contouring of hermite data. In *Proceedings of the 29th annual conference on Computer graphics and interactive techniques*, pages 339–346, 2002. **1, 3, 8**
- [18] John Kirchenbauer, Jonas Geiping, Yuxin Wen, Jonathan Katz, Ian Miers, and Tom Goldstein. A watermark for large language models. *arXiv preprint arXiv:2301.10226*, 2023. **5**
- [19] Muheng Li, Yueqi Duan, Jie Zhou, and Jiwen Lu. Diffusion-sdf: Text-to-shape via voxelized diffusion. In *Proceedings of the IEEE/CVF Conference on Computer Vision and Pattern Recognition*, pages 12642–12651, 2023. **1**
- [20] Zhaoshuo Li, Thomas Müller, Alex Evans, Russell H Taylor, Mathias Unberath, Ming-Yu Liu, and Chen-Hsuan Lin. Neuralangelo: High-fidelity neural surface reconstruction. In *Proceedings of the IEEE/CVF Conference on Computer Vision and Pattern Recognition*, pages 8456–8465, 2023. **1, 2**
- [21] David B Lindell, Dave Van Veen, Jeong Joon Park, and Gordon Wetzstein. Bacon: Band-limited coordinate networks for multiscale scene representation. In *Proceedings of the IEEE/CVF conference on computer vision and pattern recognition*, pages 16252–16262, 2022. **1, 2**
- [22] P. Lindstrom et al. Fast and memory efficient polygonal simplification. In *IEEE Vis*, pages 279–286. IEEE, 1998. **8**
- [23] Steven Liu, Xiuming Zhang, Zhoutong Zhang, Richard Zhang, Jun-Yan Zhu, and Bryan Russell. Editing conditional radiance fields. In *Proceedings of the IEEE/CVF international conference on computer vision*, pages 5773–5783, 2021. **4**
- [24] Zhengzhe Liu, Yi Wang, Xiaojuan Qi, and Chi-Wing Fu. Towards implicit text-guided 3d shape generation. In *Proceed-*

- ings of the *IEEE/CVF Conference on Computer Vision and Pattern Recognition*, pages 17896–17906, 2022. 1
- [25] William E Lorensen and Harvey E Cline. Marching cubes: A high resolution 3d surface construction algorithm. In *Seminal graphics: pioneering efforts that shaped the field*, pages 347–353. 1998. 1, 3, 6, 8
- [26] Ziyuan Luo, Qing Guo, Ka Chun Cheung, Simon See, and Renjie Wan. Copyrnerf: Protecting the copyright of neural radiance fields. In *Proceedings of the IEEE/CVF International Conference on Computer Vision*, pages 22401–22411, 2023. 2, 3
- [27] Lars Mescheder, Michael Oechsle, Michael Niemeyer, Sebastian Nowozin, and Andreas Geiger. Occupancy networks: Learning 3d reconstruction in function space. In *Proceedings of the IEEE/CVF conference on computer vision and pattern recognition*, pages 4460–4470, 2019. 2
- [28] Mateusz Michalkiewicz, Jhony K Pontes, Dominic Jack, Mahsa Baktashmotlagh, and Anders Eriksson. Implicit surface representations as layers in neural networks. In *Proceedings of the IEEE/CVF International Conference on Computer Vision*, pages 4743–4752, 2019. 2, 3
- [29] Ben Mildenhall, Pratul P Srinivasan, Matthew Tancik, Jonathan T Barron, Ravi Ramamoorthi, and Ren Ng. Nerf: Representing scenes as neural radiance fields for view synthesis. *Communications of the ACM*, 65(1):99–106, 2021. 2
- [30] Paritosh Mittal, Yen-Chi Cheng, Maneesh Singh, and Shubham Tulsiani. Autosdf: Shape priors for 3d completion, reconstruction and generation. In *Proceedings of the IEEE/CVF Conference on Computer Vision and Pattern Recognition*, pages 306–315, 2022. 1
- [31] Thomas Müller, Alex Evans, Christoph Schied, and Alexander Keller. Instant neural graphics primitives with a multi-resolution hash encoding. *ACM Transactions on Graphics (TOG)*, 41(4):1–15, 2022. 1, 2
- [32] Gregory M Nielson. Dual marching cubes. In *IEEE visualization 2004*, pages 489–496. IEEE, 2004. 1, 3, 8
- [33] 1 Ryutarou Ohbuchi, 1 Akio Mukaiyama, and 2 Shigeo Takahashi. A frequency-domain approach to watermarking 3d shapes. In *Computer graphics forum*, pages 373–382. Wiley Online Library, 2002. 1, 2
- [34] Ryutarou Ohbuchi, Shigeo Takahashi, Takahiko Miyazawa, and Akio Mukaiyama. Watermarking 3d polygonal meshes in the mesh spectral domain. In *Graphics interface*, pages 9–17, 2001. 2
- [35] Jeong Joon Park, Peter Florence, Julian Straub, Richard Newcombe, and Steven Lovegrove. DeepSDF: Learning continuous signed distance functions for shape representation. In *Proceedings of the IEEE/CVF conference on computer vision and pattern recognition*, pages 165–174, 2019. 1, 2, 3
- [36] Fei Peng, Bo Long, and Min Long. A general region nesting-based semi-fragile reversible watermarking for authenticating 3d mesh models. *IEEE transactions on circuits and systems for video technology*, 31(11):4538–4553, 2021. 6, 7
- [37] Fei Peng, Tongxin Liao, and Min Long. A semi-fragile reversible watermarking for authenticating 3d models in dual domains based on variable direction double modulation. *IEEE Transactions on Circuits and Systems for Video Technology*, 32(12):8394–8408, 2022. 2
- [38] Songyou Peng, Michael Niemeyer, Lars Mescheder, Marc Pollefeys, and Andreas Geiger. Convolutional occupancy networks. In *Computer Vision–ECCV 2020: 16th European Conference, Glasgow, UK, August 23–28, 2020, Proceedings, Part III 16*, pages 523–540. Springer, 2020. 2
- [39] Marie-Julie Rakotosaona, Fabian Manhardt, Diego Martin Arroyo, Michael Niemeyer, Abhijit Kundu, and Federico Tombari. Nerfmeshing: Distilling neural radiance fields into geometrically-accurate 3d meshes. *arXiv preprint arXiv:2303.09431*, 2023. 1, 2
- [40] Aditya Sanghi, Hang Chu, Joseph G Lambourne, Ye Wang, Chin-Yi Cheng, Marco Fumero, and Kamal Rahimi Malekshan. Clip-forge: Towards zero-shot text-to-shape generation. In *Proceedings of the IEEE/CVF Conference on Computer Vision and Pattern Recognition*, pages 18603–18613, 2022. 1
- [41] Tianchang Shen, Jun Gao, Kangxue Yin, Ming-Yu Liu, and Sanja Fidler. Deep marching tetrahedra: a hybrid representation for high-resolution 3d shape synthesis. *Advances in Neural Information Processing Systems*, 34:6087–6101, 2021. 1, 3, 8
- [42] Tianchang Shen, Jacob Munkberg, Jon Hasselgren, Kangxue Yin, Zian Wang, Wenzheng Chen, Zan Gojcic, Sanja Fidler, Nicholas Sharp, and Jun Gao. Flexible isosurface extraction for gradient-based mesh optimization. *ACM Transactions on Graphics (TOG)*, 42(4):1–16, 2023. 1, 3
- [43] Vincent Sitzmann, Julien Martel, Alexander Bergman, David Lindell, and Gordon Wetzstein. Implicit neural representations with periodic activation functions. *Advances in neural information processing systems*, 33:7462–7473, 2020. 1, 2, 3, 4, 6
- [44] David Stutz and Andreas Geiger. Learning 3d shape completion under weak supervision. *International Journal of Computer Vision*, 128:1162–1181, 2020. 6
- [45] Yuan-Yu Tsai. Separable reversible data hiding for encrypted three-dimensional models based on spatial subdivision and space encoding. *IEEE transactions on multimedia*, 23:2286–2296, 2020. 6, 7
- [46] Yuan-Yu Tsai and Hong-Lin Liu. Integrating coordinate transformation and random sampling into high-capacity reversible data hiding in encrypted polygonal models. *IEEE Transactions on Dependable and Secure Computing*, 2022. 1, 2, 3
- [47] Hongyi Xu, Thiemo Alldieck, and Cristian Sminchisescu. H-nerf: Neural radiance fields for rendering and temporal reconstruction of humans in motion. *Advances in Neural Information Processing Systems*, 34:14955–14966, 2021. 1, 2
- [48] Guandao Yang, Serge Belongie, Bharath Hariharan, and Vladlen Koltun. Geometry processing with neural fields. *Advances in Neural Information Processing Systems*, 34:22483–22497, 2021. 4, 5, 6
- [49] Innfarn Yoo, Huiwen Chang, Xiyang Luo, Ondrej Stava, Ce Liu, Peyman Milanfar, and Feng Yang. Deep 3d-to-2d watermarking: embedding messages in 3d meshes and extracting

- them from 2d renderings. In *Proceedings of the IEEE/CVF Conference on Computer Vision and Pattern Recognition*, pages 10031–10040, 2022. [1](#), [3](#)
- [50] Tjalling J Ypma. Historical development of the newton–raphson method. *SIAM review*, 37(4):531–551, 1995. [4](#)
- [51] Yushu Zhang, Jiahao Zhu, Mingfu Xue, Xinpeng Zhang, and Xiaochun Cao. Adaptive 3d mesh steganography based on feature-preserving distortion. *IEEE Transactions on Visualization and Computer Graphics*, 2023. [1](#), [2](#), [3](#)
- [52] Mingwu Zheng, Hongyu Yang, Di Huang, and Liming Chen. Imface: A nonlinear 3d morphable face model with implicit neural representations. In *Proceedings of the IEEE/CVF Conference on Computer Vision and Pattern Recognition*, pages 20343–20352, 2022. [1](#), [2](#)
- [53] Yi Zhou, Connelly Barnes, Jingwan Lu, Jimei Yang, and Hao Li. On the continuity of rotation representations in neural networks. In *Proceedings of the IEEE/CVF Conference on Computer Vision and Pattern Recognition*, pages 5745–5753, 2019. [5](#)
- [54] Xingyu Zhu, Guanhui Ye, Xuetao Wei, and Xiapu Luo. Wm-net: Robust deep 3d watermarking with limited data. *arXiv preprint arXiv:2307.11628*, 2023. [1](#), [3](#)